

000
001
002054
055
056003
004057
058005
006
007059
060
061008
009
010062
063
064011
012
013065
066
067

1. MVTec qualitative examples

Fig.1, 2, and 3 show each qualitative examples in each category of the MVTec anomaly detection dataset [2]. We also enumerate all the negative samples in Fig.4. Since the heat maps are normalized, high heat values obtained in some non-anomalous regions do not imply that they are predicted to be abnormal. A qualitative comparison of ARD with RD [6] is shown in Fig.5. The images in Fig.1, 2, ,3 ,4, and 5 are best viewed zoomed in.

2. Surface Anomaly Detection and One-Class Novelty Detection

Fig. 6 shows qualitative examples of ARD and RD [6] for some DAGM [17] categories to show that ARD's detection and localization accuracy for surface anomalies that are small or close to the background is superior to the previous best unsupervised surface anomaly detection method. the images in Fig.6. is best viewed zoomed in.

For Surface Anomaly Detection, We further validate the performance of the proposed model on complex textured backgrounds on the DAGM [17] dataset and report the results for each category in Tab.I and Tab.II. All experimental settings for DAGM are the same as for MVTec. The baselines of surface anomaly detection include Uniformed Student (US) [3], STPM [15], SAPDE [4], RIAD [21], PaDim [5], CutPaste [11], DRÆM [20], MKD [14] and RD [6].

For One-Class Anomaly Detection, We follow previous work on one-class anomaly detection. We use one class as training samples and the other classes as anomaly samples for detection. We use ResNet34 [7] as the backbone for the teacher and student encoders, and the models are trained for a total of 200 epochs with a batch size of 16. Query every 10 epochs and save the model. The model is optimized by Adam optimizer with learning rate of 0.001. Tab.III presents the detailed numerical results of novelty detection with training on each class of samples. The baselines in one-class anomaly detection are LSA [1], HRN [10], OC-GAN [12], DASVDD [8] and RD [6].

Anonymous AI submission

Paper ID

Our code is available at <https://github.com/ssiing/ARD>.

References

- [1] Davide Abati, Angelo Porrello, Simone Calderara, and Rita Cucchiara. Latent space autoregression for novelty detection. In *Proceedings of the IEEE/CVF conference on computer vision and pattern recognition*, pages 481–490, 2019. 1
- [2] Paul Bergmann, Kilian Batzner, Michael Fauser, David Sattlegger, and Carsten Steger. The mvtect anomaly detection dataset: a comprehensive real-world dataset for unsupervised anomaly detection. *International Journal of Computer Vision*, 129(4):1038–1059, 2021. 1, 4, 5, 6, 7, 8
- [3] Paul Bergmann, Michael Fauser, David Sattlegger, and Carsten Steger. Uninformed students: Student-teacher anomaly detection with discriminative latent embeddings. In *Proceedings of the IEEE/CVF Conference on Computer Vision and Pattern Recognition*, pages 4183–4192, 2020. 1
- [4] Niv Cohen and Yedid Hoshen. Sub-image anomaly detection with deep pyramid correspondences. *arXiv preprint arXiv:2005.02357*, 2020. 1
- [5] Thomas Defard, Aleksandr Setkov, Angelique Loesch, and Romaric Audigier. Padim: a patch distribution modeling framework for anomaly detection and localization. In *International Conference on Pattern Recognition*, pages 475–489. Springer, 2021. 1
- [6] Hanqiu Deng and Xingyu Li. Anomaly detection via reverse distillation from one-class embedding. In *Proceedings of the IEEE/CVF Conference on Computer Vision and Pattern Recognition*, pages 9737–9746, 2022. 1, 8, 9
- [7] Kaiming He, Xiangyu Zhang, Shaoqing Ren, and Jian Sun. Deep residual learning for image recognition. In *Proceedings of the IEEE conference on computer vision and pattern recognition*, pages 770–778, 2016. 1
- [8] Hadi Hojjati and Narges Armanfard. Dasvdd: Deep autoencoding support vector data descriptor for anomaly detection. *arXiv preprint arXiv:2106.05410*, 2021. 1
- [9] Jie Hu, Li Shen, and Gang Sun. Squeeze-and-excitation networks. In *Proceedings of the IEEE conference on computer vision and pattern recognition*, pages 7132–7141, 2018.

- 108 [10] Wenpeng Hu, Mengyu Wang, Qi Qin, Jinwen Ma, and
109 Bing Liu. Hrn: A holistic approach to one class learn-
110 ing. *Advances in Neural Information Processing Systems*,
111 33:19111–19124, 2020. 1 162
112 [11] Chun-Liang Li, Kihyuk Sohn, Jinsung Yoon, and Tomas
113 Pfister. Cutpaste: Self-supervised learning for anomaly de-
114 tection and localization. In *Proceedings of the IEEE/CVF*
115 *Conference on Computer Vision and Pattern Recognition*,
116 pages 9664–9674, 2021. 1 163
117 [12] Pramuditha Perera, Ramesh Nallapati, and Bing Xiang. Oc-
118 gan: One-class novelty detection using gans with constrained
119 latent representations. In *Proceedings of the IEEE/CVF Con-*
120 *fERENCE ON COMPUTER VISION AND PATTERN RECOGNITION*, pages
121 2898–2906, 2019. 1 164
122 [13] Nicolae-Cătălin Ristea, Neelu Madan, Radu Tudor Ionescu,
123 Kamal Nasrollahi, Fahad Shahbaz Khan, Thomas B Moes-
124 lund, and Mubarak Shah. Self-supervised predictive convo-
125 lutional attentive block for anomaly detection. In *Proceed-
126 ings of the IEEE/CVF Conference on Computer Vision and
127 Pattern Recognition*, pages 13576–13586, 2022. 165
128 [14] Mohammadreza Salehi, Niousha Sadjadi, Soroosh
129 Baselizadeh, Mohammad H Rohban, and Hamid R Rabiee.
130 Multiresolution knowledge distillation for anomaly de-
131 tection. In *Proceedings of the IEEE/CVF confer-
132 ence on computer vision and pattern recognition*, pages
133 14902–14912, 2021. 1 166
134 [15] Guodong Wang, Shumin Han, Errui Ding, and Di Huang.
135 Student-teacher feature pyramid matching for unsupervised
136 anomaly detection. *arXiv preprint arXiv:2103.04257*, 2021.
137 1 167
138 [16] Qilong Wang, Banggu Wu, Pengfei Zhu, Peihua Li, Wang-
139 meng Zuo, and Qinghua Hu. Eca-net: Efficient channel at-
140 tention for deep convolutional neural networks. In *Proceed-
141 ings of the 2020 IEEE/CVF Conference on Computer Vision
142 and Pattern Recognition*, IEEE, Seattle, WA, USA, pages 13–
143 19, 2020. 168
144 [17] Matthias Wieler and Tobias Hahn. Weakly supervised learn-
145 ing for industrial optical inspection. In *DAGM symposium
146 in*, 2007. 1, 3, 9 169
147 [18] Sanghyun Woo, Jongchan Park, Joon-Young Lee, and In So
148 Kweon. Cbam: Convolutional block attention module. In
149 *Proceedings of the European conference on computer vision
(ECCV)*, pages 3–19, 2018. 170
150 [19] Sergey Zagoruyko and Nikos Komodakis. Wide residual net-
151 works. *arXiv preprint arXiv:1605.07146*, 2016. 171
152 [20] Vitjan Zavrtanik, Matej Kristan, and Danijel Skočaj. Draem-
153 a discriminatively trained reconstruction embedding for sur-
154 face anomaly detection. In *Proceedings of the IEEE/CVF
155 International Conference on Computer Vision*, pages 8330–
156 8339, 2021. 1 172
157 [21] Vitjan Zavrtanik, Matej Kristan, and Danijel Skočaj. Recon-
158 struction by inpainting for visual anomaly detection. *Pattern
159 Recognition*, 112:107706, 2021. 1 173
160 174
161 175
176
177
178
179
180
181
182
183
184
185
186
187
188
189
190
191
192
193
194
195
196
197
198
199
200
201
202
203
204
205
206
207
208
209
210
211
212
213
214
215

216

270

217

271

218

272

Category	STPM	RIAD	SPADE	PaDim	DRÆM	CutPaste	MKD	RD	ARD
Class1	83.0	43.6	49.9	87.8	69.9	65.0	55.14	76.5	98.3
Class2	98.3	57.4	96.1	99.8	95.6	99.7	83.6	92.7	100
Class3	90.4	49.2	79.3	97.7	82.3	100	72.7	87.6	93.5
Class4	99.6	89.2	89.6	100	100	99.7	96.7	100	100
Class5	81.8	72.0	82.2	93.1	97.4	79.1	73.4	90.7	93.9
Class6	93.4	90.7	94.0	96.2	99.3	76.3	93.2	97.9	99.3
Class7	61.0	49.0	58.2	97.1	100	100	60.3	99.6	100
Class8	67.8	48.9	61.8	72.0	95.9	99.7	59.4	64.4	66.0
Class9	97.0	46.3	95.0	97.5	53.4	90.2	85.0	95.1	99.5
Class10	99.4	81.8	87.2	100	90.3	96.9	87.6	99.8	100
Average	87.1	62.8	79.3	94.1	88.4	90.6	76.7	90.4	95.0

229

283

Table 1. Anomaly Detection results on DAGM [17]. methods achieved for the top average AUROC(%) is highlighted in bold.

230

284

231

285

232

286

233

287

234

288

235

289

Category	US	STPM	RIAD	SPADE	PaDim	DRÆM	RD	ARD
Class1	56.3/23.4	89.6/74.4	41.7/9.5	51.3/-	90.1/77.4	62.8/46.6	92.2/87.6	93.7/91.5
Class2	77.0/61.9	98.7/95.5	70.4/34.1	53.5/-	98.8/97.7	77.6/66.6	95.4/94.5	99.2/99.0
Class3	68.8/46.3	95.2/89.5	72.7/41.9	53.0/-	96.4/92.0	77.9/62.4	94.7/88.3	93.8/88.0
Class4	67.6/37.3	99.1/97.0	93.8/81.2	44.2/-	99.5/98.1	82.1/68.0	99.3/98.1	99.6/98.6
Class5	62.7/32.0	92.6/73.1	85.4/63.9	52.6/-	96.7/83.5	79.9/64.5	90.7/88.0	96.2/89.3
Class6	54.9/20.1	92.3/76.4	85.5/63.9	52.6/-	96.9/90.1	85.4/67.4	93.8/80.1	96.8/89.4
Class7	62.5/34.4	82.3/60.2	72.2/37.0	54.7/-	92.0/84.0	81.5/70.8	95.2/92.1	96.0/93.4
Class8	61.8/32.0	89.0/62.1	53.2/15.7	50.6/-	92.5/74.1	83.5/74.2	88.4/69.6	88.3/69.9
Class9	81.4/60.3	99.1/94.0	68.5/38.5	50.3/-	99.4/95.4	83.9/63.2	99.2/97.9	99.7/99.4
Class10	81.0/67.2	98.2/94.8	92.9/82.8	57.0/-	98.9/96.5	84.1/65.4	98.9/98.1	99.2/98.5
Average	67.4/41.4	93.6/81.7	73.6/46.8	51.9/-	96.1/88.8	79.8/64.9	94.7/89.4	96.2/94.7

248

302

Table 2. Anomaly Localization results with AUROC and PRO on DAGM [17]. The top results for AUROC and PRO in bold.

249

303

250

304

251

305

252

306

253

307

Dataset	MINST/F-MINST						CIFAR-10					
	Methods	LSA	HRN	OCGAN	DASVVDD	RD	ARD	LSA	HRN	OCGAN	DASVDD	RD
0	99.3/-	99.5/92.7	99.8/85.5	99.7/91.2	99.7/92.7	99.9/93.7	73.5	77.3	75.7	68.6	88.0	89.2
1	99.9 /-	99.9 /98.5	99.9 /93.4	99.9 /99.0	99.9 /99.5	99.9 / 99.7	58.0	69.9	53.1	64.3	90.4	91.3
2	95.9/-	96.5/88.5	94.2/85.0	95.4/89.3	80.6/91.4	99.5/92.6	69.0	60.6	64.0	55.8	76.9	78.3
3	96.6/-	97.4/93.1	96.3/88.1	96.2/93.7	99.0/95.3	99.1/96.2	54.2	64.4	62.0	58.6	67.6	67.0
4	95.6/-	97.2/92.1	97.5/85.8	98.1/90.7	97.4/ 93.9	98.5/93.8	76.1	71.5	72.3	64.0	85.3	87.0
5	96.4/-	97.2/91.3	98.0/88.5	97.2/93.8	99.0/95.4	99.2/96.6	54.6	67.4	62.0	62.6	80.6	80.3
6	99.4/-	99.2/79.8	99.1/775	99.6/82.8	97.4/83.4	99.8/84.0	75.1	77.4	72.3	71.0	90.7	90.7
7	98.0/-	97.6/99.0	98.1/93.9	98.1/98.6	98.5/99.4	99.2/99.5	53.5	64.9	57.5	64.6	89.8	88.1
8	95.3/-	94.3/94.6	93.9/82.7	94.2/89.4	98.7/96.5	99.3/97.1	71.7	82.5	82.0	81.1	92.1	92.1
9	98.1/-	97.1/98.8	98.1/97.8	98.3/97.9	99.5/88.7	99.5/98.8	54.9	77.3	55.4	73.7	89.5	89.7
Average	97.4/-	97.6/92.8	97.5/87.8	97.7/92.6	96.9/93.6	99.3/95.2	64.0	71.3	65.7	66.5	85.0	85.3

266

320

Table 3. AUROC(%) results for One-Class Anomaly Detection. The top results for AUROC and PRO in bold.

267

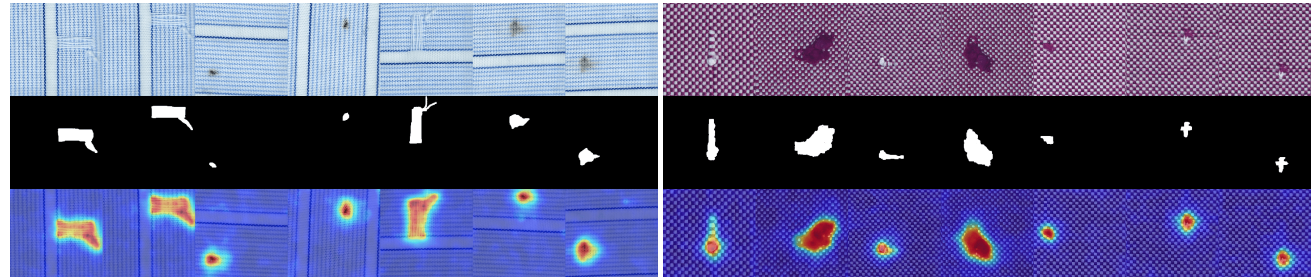
321

268

322

269

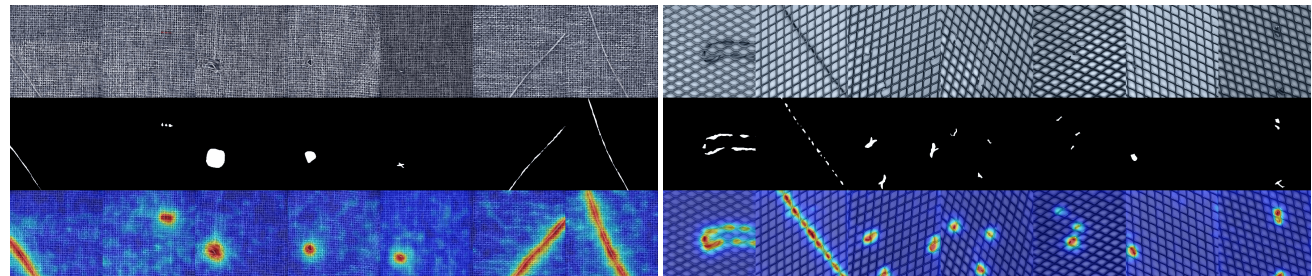
323

324
325
326
327
328
329
330378
379
380
381
382
383
384331
332
333
334
335
336
337
338
339385
386
387
388
389
390
391
392
393
394

(a) blue

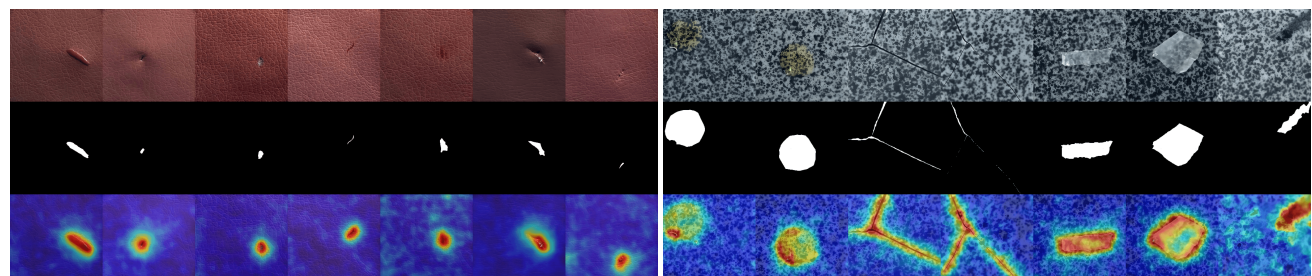
(b) red

340

341
342
343395
396
397

(c) carpet

(d) grid

344
345
346
347
348
349398
399350
351
352400
401
402
403
404
405
406
407
408
409

(e) leather

(f) tile

353
354

410

Figure 1. ARD qualitative examples for the MVTec dataset [2]. The original image, the ground truth mapthe output, and anomaly map are shown. Best viewed zoomed in.

355

411

356

412

357
358
359413
414
415360
361
362

416

363
364417
418
419

365

420

366
367421
422

368

423
424

369

425

370

426

371
372427
428

373

429
430

374

431

375

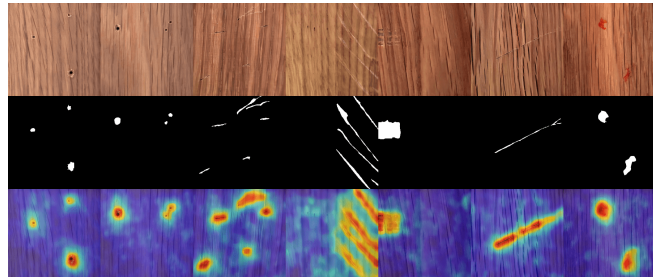
430
431

376

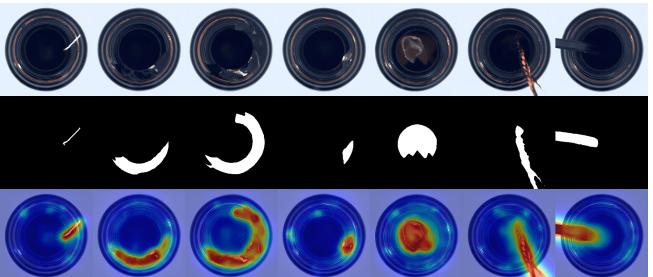
430
431

377

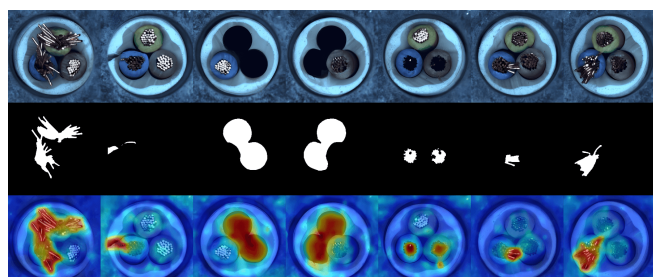
430
431

432
433
434
435
436
437
438486
487
488
489
490
491
492

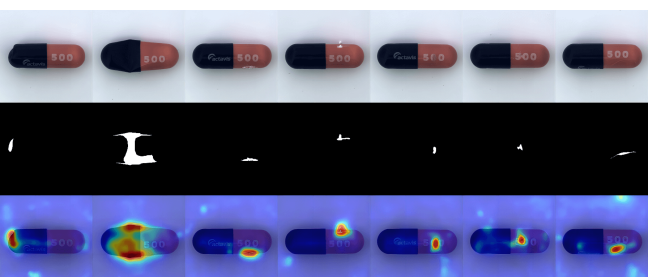
(a) wood



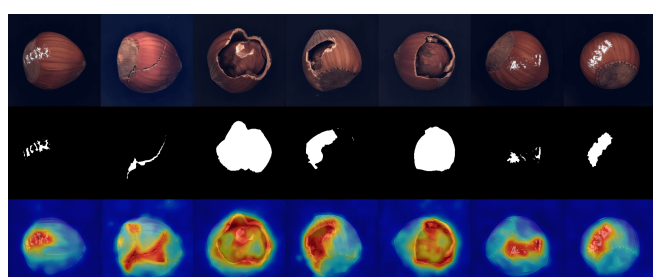
(b) bottle



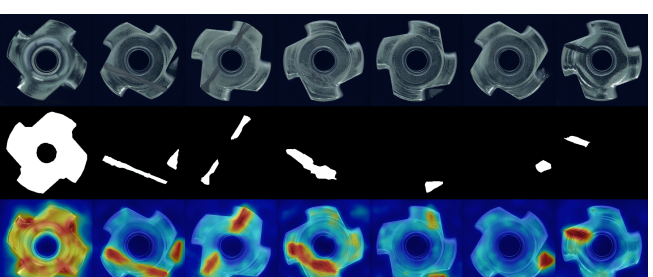
(c) cable



(d) capsule



(e) hazelnut

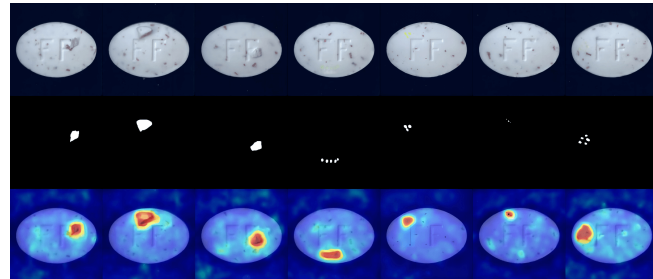


(f) metal nut

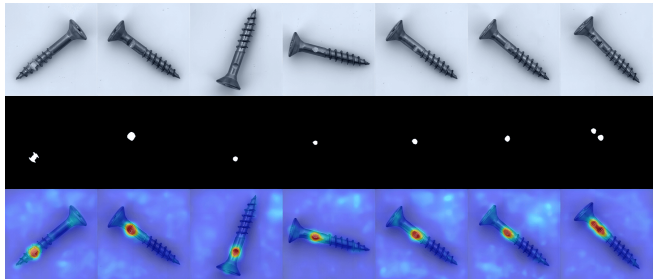
477
478528
529

Figure 2. ARD qualitative examples for the MVTec dataset [2]. The original image, the ground truth mapthe output, and anomaly map are shown. Best viewed zoomed in.

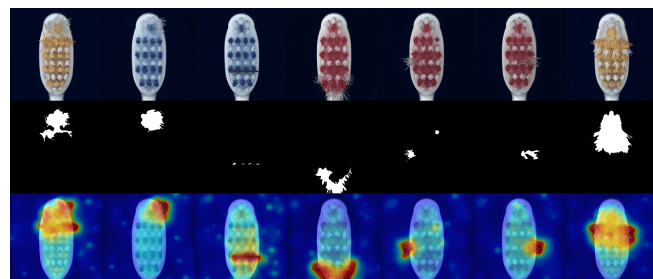
479
480
481
482
483
484
485530
531
532
533
534
535
536
537
538
539

540
541
542
543
544
545
546594
595
596
597
598
599
600

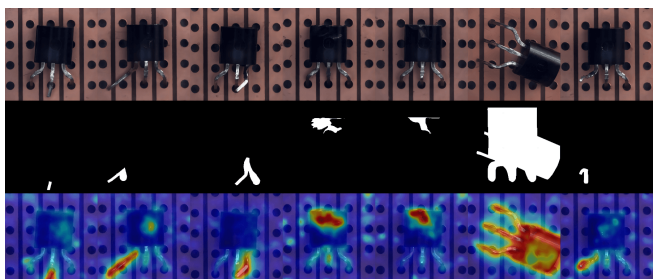
(a) pill



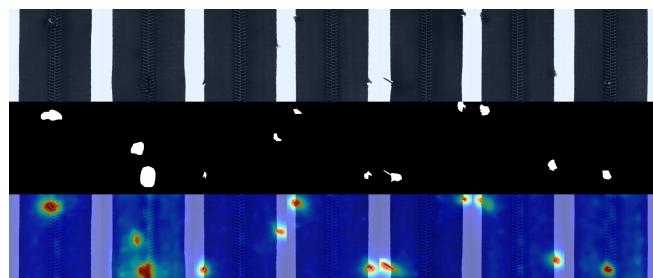
(b) screw



(c) toothbrush



(d) transistor



(e) zipper

Figure 3. ARD qualitative examples for the MVTec dataset [2]. The original image, the ground truth mapthe output, and anomaly map are shown. Best viewed zoomed in.

587
588
589
590
591
592
593639
640
641
642
643
644
645
646
647

648

649

650

651

652

653

654

655

656

657

658

659

660

661

662

663

664

665

666

667

668

669

670

671

672

673

674

675

676

677

678

679

680

681

682

683

684

685

686

687

688

689

690

691

692

693

694

695

696

697

698

699

700

701

702

703

704

705

706

707

708

709

710

711

712

713

714

715

716

717

718

719

720

721

722

723

724

725

726

727

728

729

730

731

732

733

734

735

736

737

738

739

740

741

742

743

744

745

746

747

748

749

750

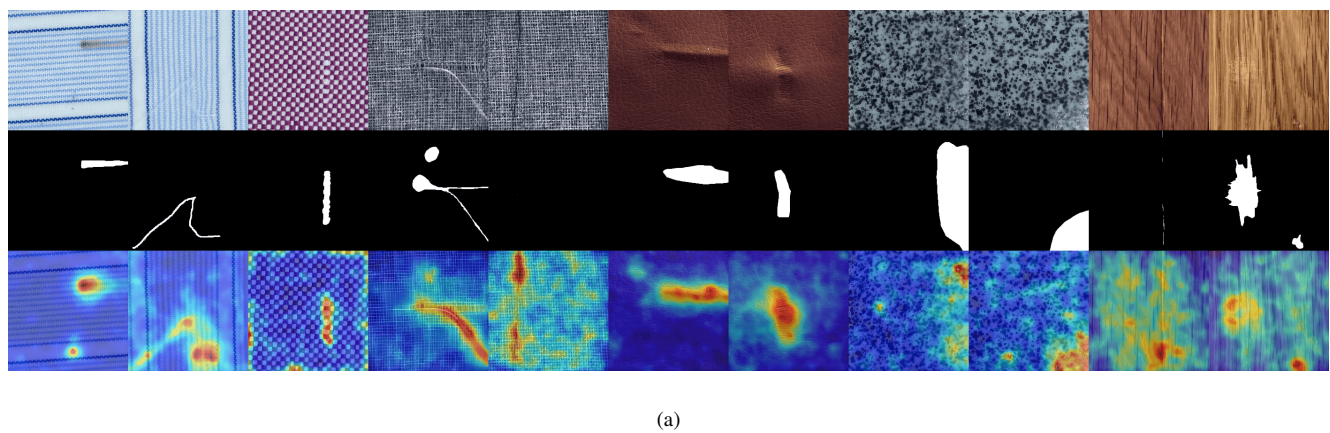
751

752

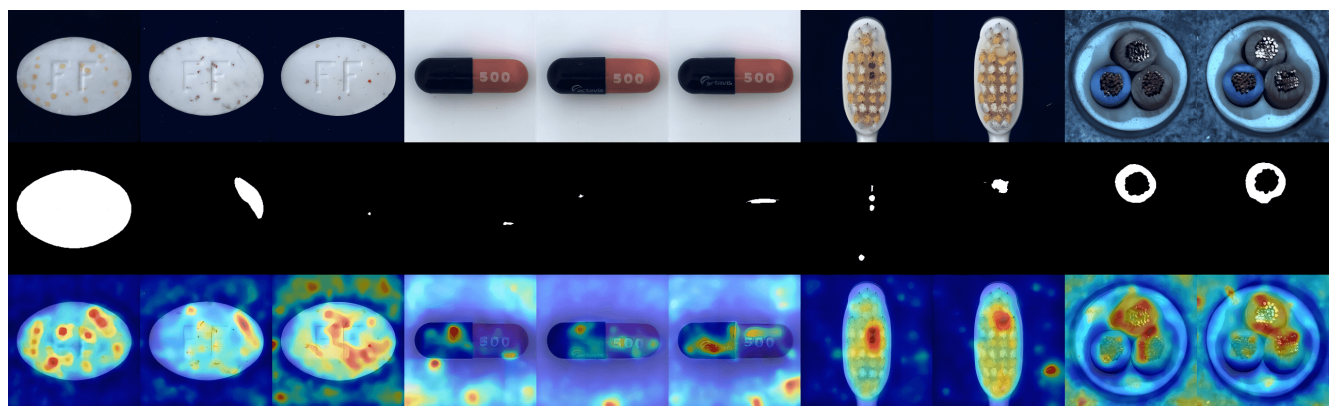
753

754

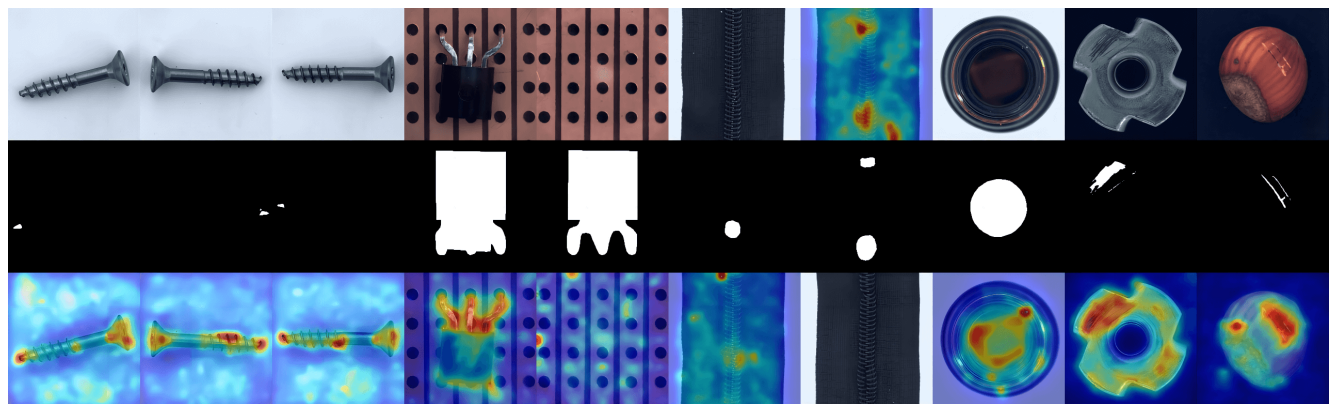
755



(a)

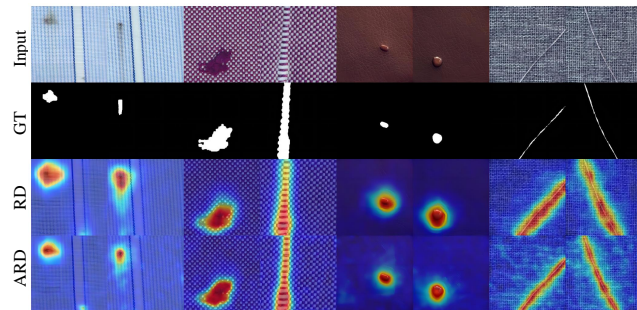


(b)

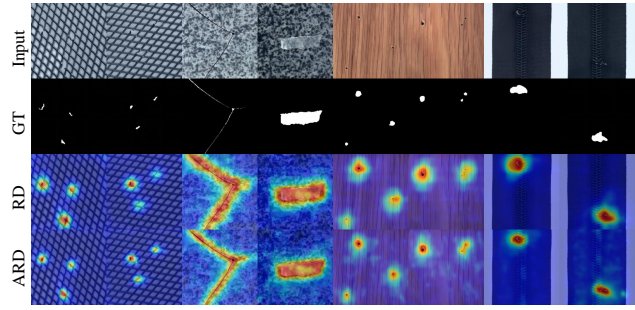


(c)

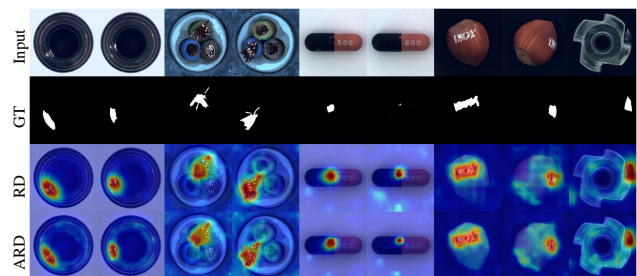
Figure 4. Negative samples of the MVTec dataset [2]. The original image Input, the ground truth map GT, and the ARD anomaly map are shown.

756
757
758
759
760
761
762
763
764
765
766
767

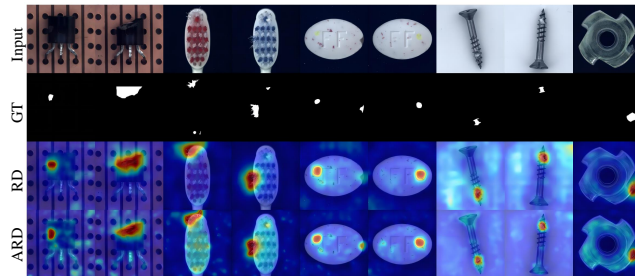
(a) blue, red, leather, and carpet



(b) grid, tile, wood, and zipper



(c) bottle, cable, capsule, hazelnut, and metal nut



(d) transistor, toothbrush, pill, screw, and metal nut

796 Figure 5. Qualitative comparison of ARD to the anomaly detection methods RD [6] on the MVTec dataset [2]. The original image (I),
797 ground truth map (GT), and the anomaly overlays for two methods are shown.
798850
851
852
853
854
855
856
857
858
859
860
861
862
863799
800
801
802
803
804
805
806
807
808
809

864
865
866
867
868
869918
919
920
921
922
923870
871
872
873
874924
925
926
927
928875
876
877
878
879929
930
931
932
933880
881
882
883
884934
935
936
937
938

885

939

886

940

887

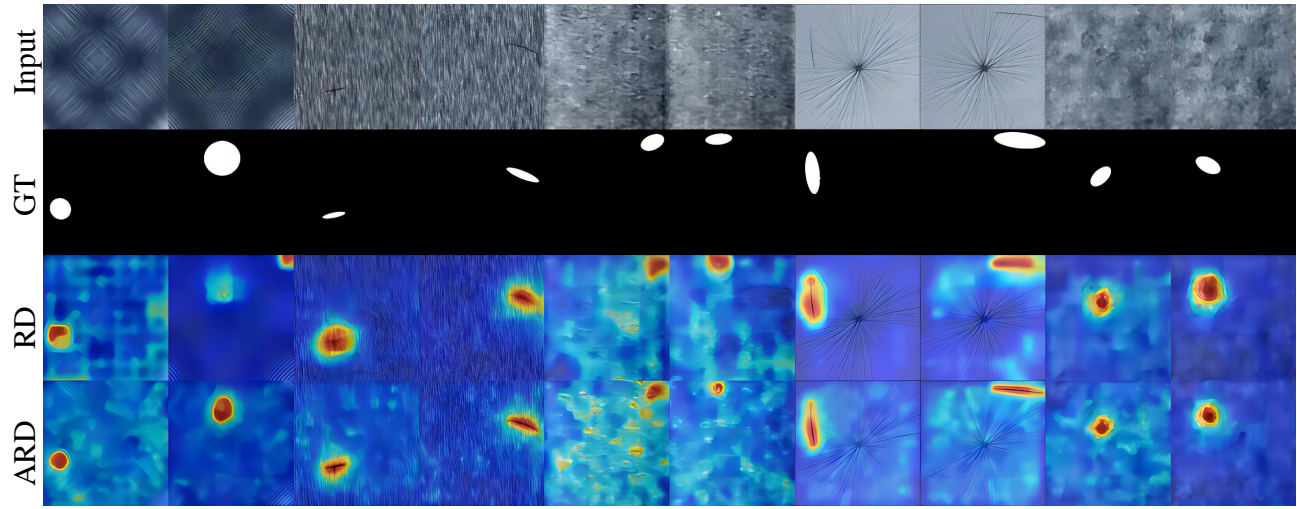
941

888

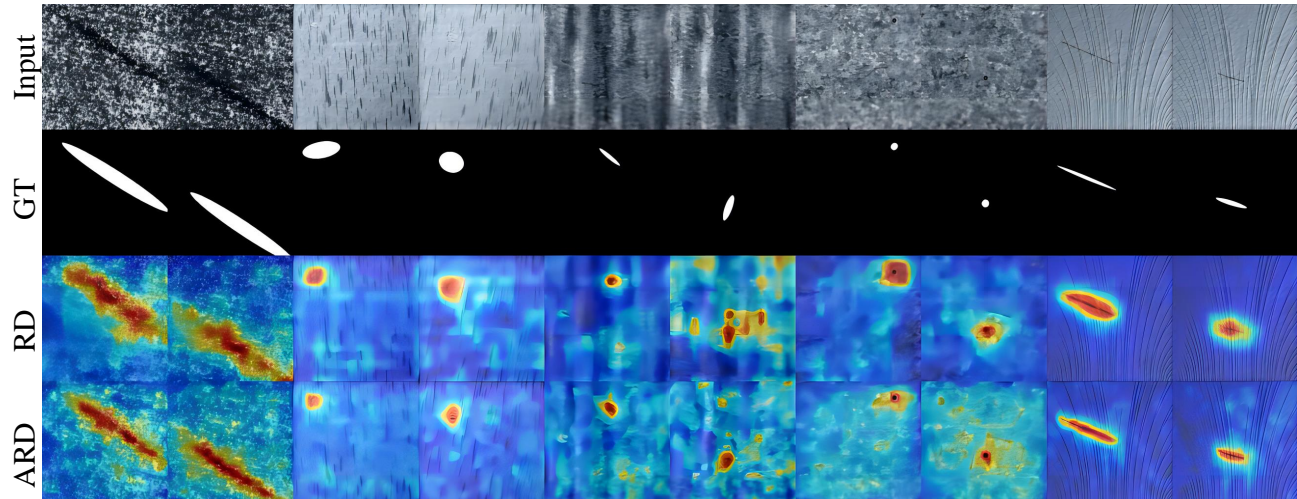
942

889

943

890
891
892
893944
945
946894
895
896
897947
948
949898
899
900
901
902
903
904
905950
951
952
953
954
955
956
957906
907
908
909958
959
960910
911
912961
962
963913
914
915
916
917964
965
966

(a)



(b)

Figure 6. Qualitative examples for the DAGM dataset [17]. The original image Input, the ground truth map GT, the anomaly map produced by RD [6], and the ARD anomaly map are shown.